# Influence of gravitational settling on turbulent droplet clustering and radar reflectivity factor

**Keigo Matsuda · Ryo Onishi · Keiko Takahashi**

**Abstract** This study investigates the influence of gravitational settling of droplets on turbulent clustering and the radar reflectivity factor. A three-dimensional direct numerical simulation (DNS) of particle-laden isotropic turbulence is performed to obtain turbulent droplet clustering data. The turbulent clustering data are then used to calculate the power spectrum of droplet number density fluctuations. The results show that the gravitational settling modulates the power spectrum more significantly as the settling becomes larger. The gravitational settling weakens the intensity of clustering at large wavenumbers for St $\leq$ 1, whereas it significantly enlarges the intensity for St $>$ 1. The dependence on the Taylor-microscale-based Reynolds number is also investigated to discuss the contribution of large-scale eddies to the settling influence. The results show that large-scale eddies modulate the small scale clustering structure of large St droplets. The increment of radar reflectivity factor due to turbulent clustering is estimated from the power spectrum for the case of St = 1.0. The

K. Matsuda
Center for Earth Information Science and Technology, Japan Agency for Marine-Earth Science and Technology (JAMSTEC), 3173-25 Showa-machi, Kanazawa-ku, Yokohama 236-0001, Japan
Tel.: +81-45-778-5833
Fax: +81-45-778-5492
E-mail: k.matsuda@jamstec.go.jp

R. Onishi
Center for Earth Information Science and Technology, Japan Agency for Marine-Earth Science and Technology (JAMSTEC), 3173-25 Showa-machi, Kanazawa-ku, Yokohama 236-0001, Japan

K. Takahashi
Center for Earth Information Science and Technology, Japan Agency for Marine-Earth Science and Technology (JAMSTEC), 3173-25 Showa-machi, Kanazawa-ku, Yokohama 236-0001, Japan

result shows that the influence of gravitational settling on the radar reflectivity factor can be significant for the case of large settling velocity droplets.

**Keywords** Isotropic turbulence · Direct numerical simulation · Particle-laden flows · Radar observation

## 1 Introduction

Radar remote sensing is one of the powerful tools for meteorological observations since it can provide two- or three-dimensional estimates of cloud microphysical properties over a large domain [24,31,11]. In radar observations, microwave is transmitted from an antenna toward a target cloud and the reflected microwave is received and analyzed. The relation between the transmitted microwave power, $P_t$, and the received microwave power, $P_r$, are given by the following radar equation:

$$P_r = \frac{P_t G^2 k_m^2 |K|^2 V}{4^5 R^4} Z,$$ (1)

where $G$ is the antenna gain, $k_m$ the microwave wavenumber, $K$ the dielectric coefficient, $V$ the measurement volume, $R$ the distance between the antenna and the clouds, and $Z$ the radar reflectivity factor ($\text{mm}^6/\text{m}^3$), which is dependent on the cloud microphysical properties. This implies that cloud properties can be estimated from $Z$.

The relation between $Z$ and cloud microphysical properties are parameterized based on the assumption of incoherent scattering, which occurs when the cloud droplets are dispersed randomly and uniformly [4]. On the other hand, when the cloud droplets are distributed nonuniformly, the scattering is classified as coherent scattering, which is often referred to as Bragg scattering. Coherent scattering by discrete particles is more specifically referred to as "particulate" Bragg scattering [20]. The radar reflectivity factor for the incoherent scattering is proportional to the sum of the scattering intensity from each droplet, while the factor for the coherent scattering is larger than the sum of the scattering intensity. This is because the nonuniform droplet distribution causes the interference of scattered microwaves, which increases the scattered microwave intensity. An important difference between incoherent and coherent scattering is the dependence of $Z$ on the microwave frequency, $f_m$: $Z$ for the incoherent scattering is independent of $f_m$, while $Z$ for the coherent scattering is dependent on $f_m$. Most studies assume that particulate Bragg scattering is insignificant in atmospheric clouds [12]. However, Knight and Miller [18,19] and Rogers and Brown [29] reported the contradicted observation results. Knight and Miller [18,19] observed significant difference between the radar reflectivity factor for two different frequency for the cases of developing cumulus clouds. Rogers and Brown [29] observed similar frequency dependence for the case of smoke plume from an industrial fire. Kostinski and Jameson [20] pointed out that coherent scattering due to turbulent droplet clustering can be a cause of

the frequency dependence. Turbulent clustering is a nonuniform spatial distribution of inertial particles in turbulence and it is often referred to as preferential concentration: inertial particles concentrate in low-vorticity and high strain-rate regions due to the centrifugal motions [22,30,33,7]. Dombrovsky and Zaichik [10] analytically estimated the influence of turbulent clustering based on a semi-analytical clustering model and indicated that the turbulent clustering considerably increases the radar reflectivity factor.

Recently, Matsuda et al. [21] have performed a three-dimensional direct numerical simulation (DNS) to obtain turbulent droplet clustering data and revealed that the influence of turbulent clustering can be a cause of significant observational errors. They briefly discussed the influence of gravitational settling, and concluded that the influence of the gravitational settling is insignificant when the ratio of the terminal velocity to the Kolmogorov velocity is smaller than 3. However, the ratio can be larger than 3 in a weak turbulent flow or for the case of large droplets or heavy solid particles, which can be observed in volcanic ash clouds: the density of volcanic ash particles can be larger than that of water (e.g., 2,400-2,600 kg/m$^3$) [32,8]. Thus, for the accurate estimate of the influence of turbulent clustering, it is necessary to improve our understanding of the influence of gravitational settling. It should be noted that many authors have investigated the influence of gravitational settling on turbulent clustering, focusing on the turbulence effect on droplet collisions [2, 1,26,34,3,27,15]. They discussed the influence of gravitational settling on the radial distribution function (RDF) at the scales smaller than the Kolmogorov scale, which is 0.5-1 mm in cumulus clouds. However, for estimating the influence on the radar reflectivity factor, $Z$, it is necessary to clarify the clustering structure at the scales close to the microwave wavelength, which is 3-100 mm.

Thus, this study investigates the influence of gravitational settling on the spatial distribution of turbulent clustering droplets and the radar reflectivity factor. A three-dimensional DNS of particle-laden isotropic turbulence is performed to obtain droplet distribution data. The droplet distribution data are then used to calculate the power spectrum of droplet number density fluctuations, which gives the increment of the radar reflectivity factor due to turbulent clustering. In this paper, first, the dependence of the power spectrum on the gravitational settling velocity is discussed for the case where the Stokes number, St, is unity (the Stokes number is the representative parameter for the particle inertia; see section 2.2). Then the Stokes number dependence and the turbulent Reynolds number dependence of the influence of gravitational settling are discussed. Finally, the influence of gravitational settling on the radar reflectivity factor is estimated using the power spectrum data.

## 2 Computational method

2.1 Air turbulence

The governing equations of the turbulent air flow are the continuity and
Navier-Stokes equations for three-dimensional incompressible flows:

$$\frac{\partial u_i}{\partial x_i} = 0, \tag{2}$$

$$\frac{\partial u_i}{\partial t} + \frac{\partial u_i u_j}{\partial x_j} = -\frac{1}{\rho_\mathrm{g}} \frac{\partial p}{\partial x_i} + \nu \frac{\partial^2 u_i}{\partial x_j \partial x_j} + F_i, \tag{3}$$

where $u_i$ is the air velocity in $i$th direction, $p$ the pressure, $\rho_\mathrm{g}$ the density
of air, $\nu$ the kinematic viscosity and $F_i$ the external force in $i$th direction.
The fourth-order central difference scheme is used for the advection term and
the second-order Runge-Kutta scheme for time integration. The velocity and
pressure are coupled by the Highly Simplified Marker And Cell (HSMAC)
method [16]. Statistically steady turbulence is generated by applying an ex-
ternal force, $F_i$, using the Reduced-Communication Forcing (RCF) method
[25], which maintains the intensity of large-scale eddies keeping high parallel
efficiency.

2.2 Droplet motions

Droplet motions were tracked by the Lagrangian method. This study assumes
that the droplet size is sufficiently smaller than the Kolmogorov scale and
that the density ratio of the droplet to the surrounding air is much larger than
unity [23,17]. The governing equation is

$$\frac{dv_i}{dt} = -\frac{f}{\tau_\mathrm{p}} \left( v_i - u_i \right) + g_i, \tag{4}$$

where $v_i$ is the droplet velocity in $i$th direction, $g_i$ the gravitational acceleration
in $i$th direction and $\tau_\mathrm{p}$ the droplet relaxation time defined as

$$\tau_\mathrm{p} = \frac{\rho_\mathrm{p}}{\rho_\mathrm{g}} \frac{d_\mathrm{p}^2}{18\nu}, \tag{5}$$

where $\rho_\mathrm{p}$ is the density of water and $d_\mathrm{p}$ the droplet diameter. $f$ is the correction
factor for the drag force. For the Stokes drag, $f$ is unity, whereas, for the
nonlinear drag, $f$ is given by

$$f = 1 + 0.15 \mathrm{Re}_\mathrm{p}^{0.687}, \tag{6}$$

where $\mathrm{Re}_\mathrm{p}$ is the particle Reynolds number defined as $\mathrm{Re}_\mathrm{p} = d_\mathrm{p}|\mathbf{v}-\mathbf{u}|/\nu$ [9]. For
the case of $\mathrm{Re}_\mathrm{p} \ll 1$, $f$ is close to unity. Turbulence modulation and collisions
between droplets are neglected since cloud droplets are typically dilute.

## 2.3 Computational conditions

The computational domain was set to a cube with edge length of $2\pi L_0$, where $L_0$ is the representative length scale. Periodic boundary conditions were applied in all three directions. The domain was discretized uniformly in to $N_{\mathrm{grid}}^3$ grid points. The DNS was performed for two turbulent flows with different values of the Taylor-microscale-based Reynolds number $\mathrm{Re}_\lambda \equiv u' l_\lambda / \nu$, where $u'$ is the RMS value of the velocity fluctuation and $l_\lambda$ the Taylor microscale: $\mathrm{Re}_\lambda = 126$ and 204 by setting $N_{\mathrm{grid}} = 256$ and 512, respectively. The kinematic viscosity was set to $1.5 \times 10^{-5}$ m$^2$/s.

The number of droplets, $N_{\mathrm{p}}$, was set to $8 \times 10^6$ and $1.5 \times 10^7$ for $\mathrm{Re}_\lambda = 126$ and 204, respectively. The ratio of the droplet density to the air density, $\rho_{\mathrm{p}}/\rho_{\mathrm{a}}$, was set to 840. The Stokes number, St, defined as the ratio of $\tau_{\mathrm{p}}$ to the Kolmogorov time $\tau_\eta \equiv (\nu/\epsilon)^{1/2}$, where $\epsilon$ is the energy dissipation rate, was set to 0.2, 0.5, 1.0, 2.0 and 5.0. The gravitational acceleration, $g$, was set to 9.8 m/s$^2$ and applied in $-x$ direction; that is, $g_i = -g\delta_{i1}$. There are several nondimensional parameters to represent gravitational effect: e.g., the Froude number $\mathrm{Fr} \equiv \epsilon^{3/4}/(\nu^{1/4}g)$ and the nondimensional terminal velocities $S_{\mathrm{v}} \equiv v_{\mathrm{T}}/u_\eta$ and $\Sigma_{\mathrm{v}} \equiv v_{\mathrm{T}}/u'$, where $v_{\mathrm{T}}$ is the terminal velocity and $u_\eta \equiv (\nu\epsilon)^{1/4}$ the Kolmogorov velocity [33, 14, 34, 3]. The terminal velocity, $v_{\mathrm{T}}$, is given by $\tau_{\mathrm{p}}g/f_{\mathrm{T}}$, where $f_{\mathrm{T}}$ is the correction factor, $f$, for the case of $|\mathbf{v} - \mathbf{u}| = v_{\mathrm{T}}$. Note that the relation among St, Fr and $S_{\mathrm{v}}$ are given by $S_{\mathrm{v}} = \mathrm{St}/(f_{\mathrm{T}}\mathrm{Fr})$. Table 1 shows the computational settings. For the case of Re204St1g-L, the Stokes drag was applied for the droplet motion to eliminate the influence of the settling velocity on the drag coefficient; i.e., $f = f_{\mathrm{T}} = 1$. The nonlinear drag was applied for the other cases. For the Stokes linear drag case, $v_{\mathrm{T}}$ (as well as $S_{\mathrm{v}}$) is larger than that for the nonlinear drag case. This is because the effective relaxation time, $\tau_p^* \equiv \tau_{\mathrm{p}}/\langle f \rangle \approx \tau_p/f_{\mathrm{T}}$, is larger than that of the nonlinear drag case. Thus, the settling influence observed for the Stokes drag case can be used to estimate the influence for the nonlinear drag cases with the same values of $S_{\mathrm{v}}$ and the effective Stokes number, $\mathrm{St}^* \equiv \tau_{\mathrm{p}}^*/\tau_\eta$ [33, 1]. In order to obtain the reference data for every cases, this study also performed DNSs under the absence of gravity, where Fr is infinity and $S_{\mathrm{v}}$ and $\Sigma_{\mathrm{v}}$ are zero.

## 3 Radar reflectivity factor

The microwave scattering by cloud droplets can be approximated as the Rayleigh scattering, which is valid for the case where the scattering particle size is sufficiently smaller than the wavelength. Since the intensity of Rayleigh scattering is proportional to the sixth power of the droplet diameter, $d_{\mathrm{p}}$, the radar reflectivity factor for the randomly- and uniformly-located monodispersed droplets, $Z_{\mathrm{random}}$, is given by

$$Z_{\mathrm{random}} = d_{\mathrm{p}}^6 n_{\mathrm{p}}, \tag{7}$$

**Table 1** Computational settings.

| Case | $L_0$ (m) | $Re_\lambda$ | St | Fr | $S_v$ | $\Sigma_v$ |
|---|---|---|---|---|---|---|
| Re204St1g-L | 0.0400 | 204 | 1.0 | 0.731 | 1.36 | 0.188 |
| | 0.0500 | | | 0.369 | 2.68 | 0.369 |
| | 0.0682 | | | 0.145 | 6.79 | 0.936 |
| | 0.0800 | | | 0.0900 | 11.0 | 1.51 |
| | 0.0966 | | | 0.0510 | 19.3 | 2.66 |
| Re204St02g-NL | 0.0682 | 204 | 0.20 | 0.145 | 1.32 | 0.182 |
| Re204St05g-NL | | | 0.50 | | 3.17 | 0.437 |
| Re204St1g-NL | | | 1.0 | | 5.98 | 0.824 |
| Re204St2g-NL | | | 2.0 | | 10.8 | 1.49 |
| Re204St5g-NL | | | 5.0 | | 21.6 | 2.98 |
| Re126St02g-NL | 0.0351 | 126 | 0.20 | 0.146 | 1.33 | 0.233 |
| Re126St05g-NL | | | 0.50 | | 3.19 | 0.560 |
| Re126St1g-NL | | | 1.0 | | 6.01 | 1.05 |
| Re126St2g-NL | | | 2.0 | | 10.8 | 1.90 |
| Re126St5g-NL | | | 5.0 | | 21.7 | 3.80 |

where $n_p$ is the droplet number density. On the other hand, the radar reflectivity factor for monodispersed clustering droplets, $Z_{cluster}$, is given by the following equation [12,21]:

$$Z_{cluster} = Z_{random} + \frac{2\pi^2 d_p^6}{\kappa^2} E_{np}(\kappa), \qquad (8)$$

where $\kappa$ is the magnitude of the difference vector between the incident and scattered wavenumber vectors, $\mathbf{k}_{inc}$ and $\mathbf{k}_{sca}$, respectively; that is, $\kappa = |\mathbf{k}_{inc} - \mathbf{k}_{sca}|$. Since the radar antenna receives backward scattering, $\kappa$ is given by $2k_m$. The power spectrum of droplet number density fluctuations, $E_{np}(k)$, represents the intensity of clustering for wavenumber $k$. It should be noted that Eq. (8) assumes isotropy of turbulent clustering. $E_{np}(k)$ is closely related to the radial distribution function (RDF), $g(r)$: $E_{np}(k)$ can be obtained by the Fourier transform of $[g(r) - 1]$ [21]. $E_{np}(k)$ can also be obtained directly from the DNS data: this study adopts this straightforward way.

$$E_{np}(k) = \frac{1}{\Delta k} \sum_{k-\Delta k/2 \leq k < k+\Delta k/2} \widetilde{\Phi}(\mathbf{k}), \qquad (9)$$

$$\widetilde{\Phi}(\mathbf{k}) = \frac{1}{L_0^3} \langle \widetilde{n_p}(\mathbf{k}) \widetilde{n_p}(-\mathbf{k}) \rangle, \qquad (10)$$

where $\widetilde{\Phi}(\mathbf{k})$ is the spectral density function and $\mathbf{k}$ the wavenumber vector which satisfies $k = |\mathbf{k}|$. The angle brackets represent the ensemble average. $\widetilde{n_p}(\mathbf{k})$ is the Fourier coefficient of the spatial droplet number density distribution $n_p(\mathbf{x})$, where $n_p(\mathbf{x})$ is given by

$$n_p(\mathbf{x}) = \sum_{j=1}^{N_p} \delta(\mathbf{x} - \mathbf{x}_{p,j}), \qquad (11)$$

where $\mathbf{x}_{\mathrm{p},j}$ is the position of $j$th droplet, $N_{\mathrm{p}}$ the total number of droplets, and $\delta(\mathbf{x})$ the Dirac delta function. The Fourier coefficients of Eq. (11) are then given by

$$\widetilde{n_{\mathrm{p}}}(\mathbf{k}) = \frac{1}{(2\pi)^3} \sum_{j=1}^{N_{\mathrm{p}}} \exp(-i\mathbf{k} \cdot \mathbf{x}_{\mathrm{p},j}). \tag{12}$$

Substitution of Eq. (12) into Eq. (10) yields the equation for calculating $\widetilde{\Phi}(\mathbf{k})$ [21]. $E_{\mathrm{np}}(k)$ was obtained by summing the $\widetilde{\Phi}(\mathbf{k})$ values calculated for discrete wavenumber vectors, $\mathbf{k}$, located between the spherical surfaces with radii of $k - \Delta k/2$ and $k + \Delta k/2$, where $\Delta k$ was set to $1/L_0$. It should be noted that $N_{\mathrm{p}} \times N_{\mathrm{k}}$ calculations are required for obtaining a power spectrum, $E_{\mathrm{np}}(k)$, where $N_{\mathrm{k}}$ is the number of discrete wavenumber vectors, $\mathbf{k}$. In order to reduce the computational cost, we chose 19 representative wavenumbers, giving $kL_0$ values of 1, 2, 3, 4, 6, 8, 12, 16, 24, 32, 48, 64, 96, 128, 192, 256, 384, 512, and 768. These 19 values of $k$ cover the wavenumber range more or less uniformly on a log scale.

## 4 Results and discussion

### 4.1 Turbulent clustering of droplets with St = 1.0

Figure 1 shows the spatial distributions of droplets for the case of St = 1.0 at $\mathrm{Re}_\lambda$ = 204 (Re204St1g-L). The droplets in the range of $0 < z < 4l_\eta$, where $l_\eta \equiv (\nu^3/\epsilon)^{1/4}$ is the Kolmogorov scale, are drawn. Void areas and fine clustering structure are clearly observed for the case of $S_{\mathrm{v}} = 0$. The clustering structure for $S_{\mathrm{v}} = 2.68$ is similar to that for $S_{\mathrm{v}} = 0$. For large $S_{\mathrm{v}}$, droplet clusters are extended in vertical direction; i.e., the vertical scales of void scales become larger compared with the horizontal scales as $S_{\mathrm{v}}$ increases. This vertically-extended clustering is corresponding to the nearly-two-dimensional "curtain shape" clustering, which was observed by Woittiez [34] and some other authors [3, 27].

Figure 2 shows the power spectra of droplet number density fluctuations, $E_{\mathrm{np}}(k)$, for the case of Re204St1g-L. The horizontal and vertical axes are normalized by using $l_\eta$ and $\langle n_{\mathrm{p}} \rangle$. The arrow indicates the wavenumber range relevant to radar observations, $0.05 < kl_\eta < 4.0$ [21]. As the gravitational droplet settling weakens the clustering intensity at large wavenumbers, whereas it strengthens at small wavenumbers. The weakening at large wavenumbers according to the increase of $S_{\mathrm{v}}$ indicates that settling weakens small-scale clustering [2, 1, 34]. The strengthening at small wavenumbers indicates a stronger large-scale clustering associated with the enlarged vertical void scales observed in Figure 1.
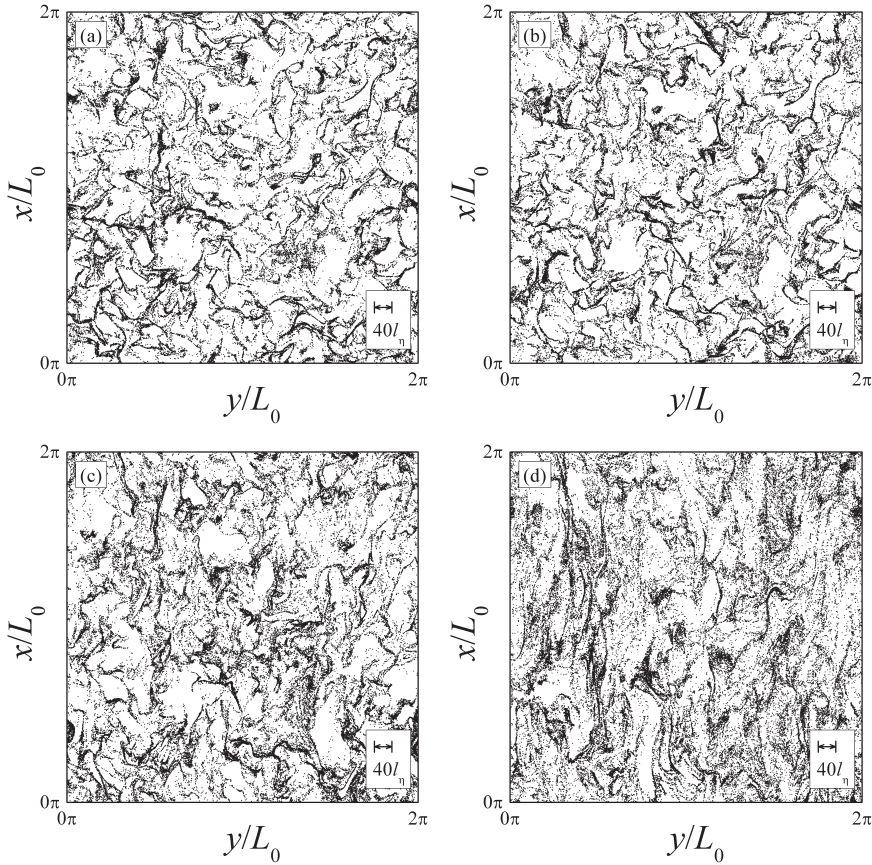
**Fig. 1** Spatial droplet distributions for St = 1.0 and (a) $S_v = 0$, (b) 2.68, (c) 6.79 and (d) 19.3 at $Re_\lambda = 204$. Droplets in the range of $0 < z < 4l_\eta$ are drawn, where $l_\eta$ is the Kolmogorov scale.

## 4.2 Stokes number dependence of turbulent clustering

The Stokes number dependence of $E_{np}(k)$ has been investigated by performing DNSs for St ranging from 0.2 (Re204St02g-NL) to 0.5 (Re204St5g-NL). Figure 3 shows the spatial distributions of droplets for St = 0.5, 2.0 and 5.0 at $Re_\lambda = 204$ under the conditions of Fr = $\infty$ and 0.145. The droplets located in the range of $0 < z < 4l_\eta$ are drawn. Note that these temporal slice of spatial droplet distributions were obtained at the same time step; i.e., the background turbulent flow fields were identical. For the case of St = 0.5, the spatial distribution of droplets for Fr = 0.145 is similar to that for Fr = $\infty$: the locations of clusters and void areas for Fr = 0.145 are corresponding to those of Fr = $\infty$. For the case of St = 0.2, the spatial distribution for Fr = 0.145 is also similar to that of Fr = $\infty$ (not shown). For the cases of St = 2.0 and 5.0, the clustering structure for Fr = 0.145 is clearly different from that for Fr = $\infty$:
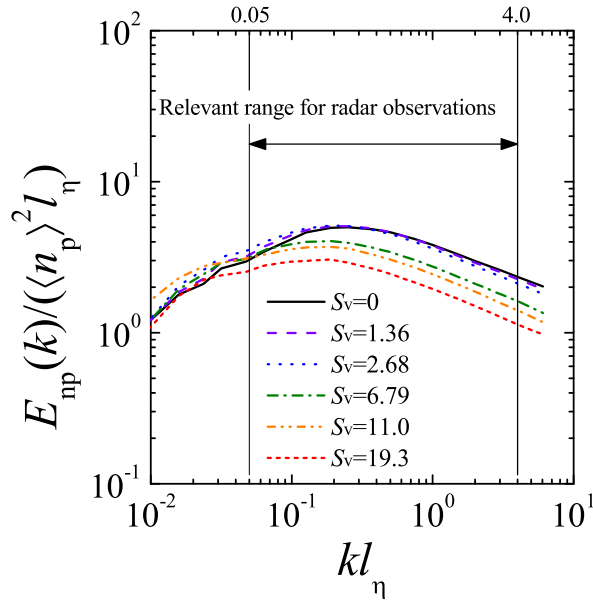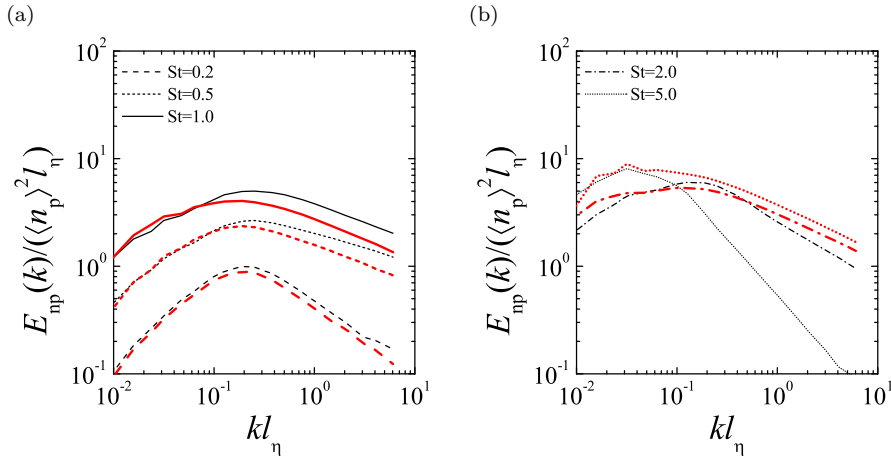
**Fig. 2** Power spectra of number density fluctuations for turbulent clustering droplets under the presence of gravity for the case of St = 1 at $\mathrm{Re}_\lambda = 204$.

for Fr = $\infty$, small-scale clusters and void areas become less clear and large-scale void areas become more prominent as St increases; on the other hand, for Fr = 0.145, the clusters become more extended in the vertical direction as St increases. These influences of gravitational settling are similar to those for St = 1.0 in Figure 1: e.g., the vertically-extended clustering in Figure 3(d) is similar to that in Figure 1(d), where the $S_v$ value is close to that of Figure 3(d). However, large-scale void areas in Figure 3(d) are more prominent than those in Figure 1(d). This difference is attributed to the different St.

Figure 4 shows the power spectrum of number density fluctuations, $E_{\mathrm{np}}(k)$, for Fr = $\infty$ and 0.145. The normalization of the horizontal and vertical axes is identical to that for Figure 2. For the case of St < 1, the power spectrum for Fr = 0.145 is lower than that for Fr = $\infty$ at large wavenumbers. The difference becomes smaller as St decreases, where $S_v$ decreases as well. The decrease of the spectrum for St ≤ 1.0 is due to the decrease of droplet-turbulence interaction time [2,34]: the gravitational settling reduces the droplet residential time in an eddy, and decreases the production of clusters. For the case of St > 1, the power spectrum for Fr = 0.145 is higher than that for Fr = $\infty$ at large wavenumbers. This enhancement is clearly observed for the case of St = 5.0: the power spectrum becomes higher for the wavenumbers larger than the peak location, showing a gentler slope. For St = 2.0, the settling influence is intermediate: the spectrum becomes lower around the peak, whereas it becomes higher for the lager wavenumbers, where the slope becomes gentler. Similar enhancement of turbulent clustering was reported by some research groups [34,3,
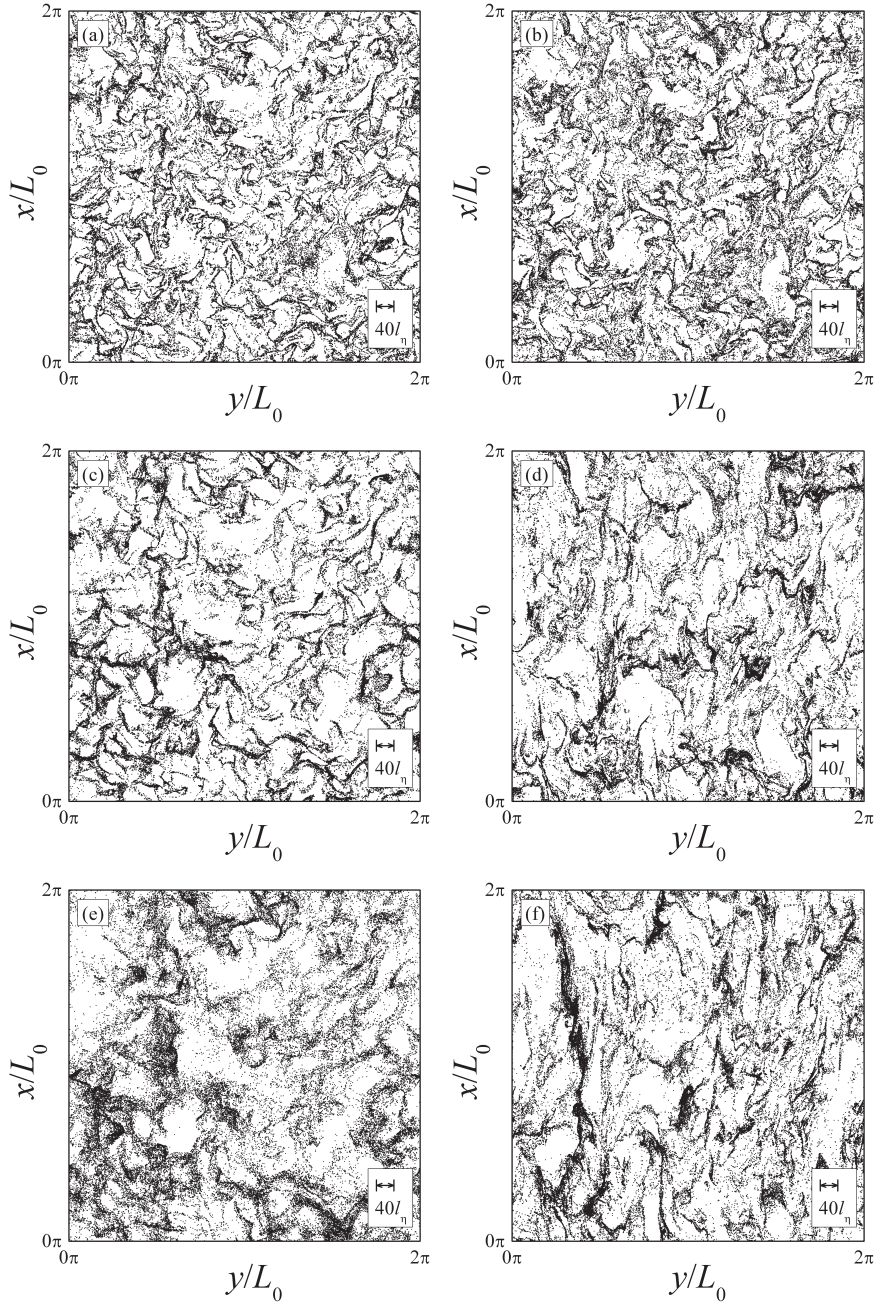
**Fig. 3** Spatial droplet distributions in turbulence for (a) St = 0.5 and $S_v = 0$ (Fr = $\infty$), (b) St = 0.5 and $S_v = 3.17$ (Fr = 0.145), (c) St = 2.0 and $S_v = 0$ (Fr = $\infty$), (d) St = 2.0 and $S_v = 10.8$ (Fr = 0.145), (e) St = 5.0 and $S_v = 0$ (Fr = $\infty$), and (f) St = 5.0 and $S_v = 21.6$ at $Re_\lambda = 204$. Droplets in the range of $0 < z < 4l_\eta$ are drawn.

(a)

(b)



**Fig. 4** Power spectra of number density fluctuations considering gravitational settling for the case of (a) St $\leq 1$ and (b) St $> 1$ at Re$_\lambda = 204$. Black and red lines indicate the spectra for the cases of Fr $= \infty$ and 0.145, respectively.

27]. They focused on the scales smaller than $l_\eta$ but, in Figure 4, we can observe the multiscale feature of the enhancement of turbulent clustering. The St dependence of the spectrum for St $> 1.0$ can be explained by a framework of the scale-dependent clustering mechanism [13,35]. Under the absence of gravity, large-scale eddies preferentially concentrate large St droplets, and small-scale eddies destroy the droplet concentration by uncorrelated stirring. On the other hand, under the presence of gravity, large-scale eddies concentrate the droplets as well, but small-scale eddies do not diffuse the concentrated droplets. This is because large St droplets have large settling velocities and, thus, they are insensitive to stirring of small-scale eddies. This scale-dependent mechanism is supported by the St dependence of the slope of the power spectrum at large wavenumbers. For Fr $= \infty$, the slope becomes steeper rapidly as St increases, indicating decorrelation of droplets in small scale. On the other hand, for Fr $= 0.145$, the relatively-gentle slope remains against the increase of St, indicating the insensitivity to the velocity fluctuation in small-scale. The insensitivity of the rapidly-settling particles is also discussed in the recent work of Gustavsson et al. [15].

In order to discuss the contribution of large-scale eddies to the settling influence, the power spectra have been calculated from the DNS data for the cases of Re$_\lambda = 126$. For these cases, where Fr $= 0.146$, the energy dissipation rate ($\epsilon = 397$ cm$^2$/s$^3$) was close to that for the cases of Re$_\lambda = 204$, where Fr $= 0.145$ ($\epsilon = 395$ cm$^2$/s$^3$). Thus, the nondimensional parameters based on the Kolmogorov-scaling values for Re$_\lambda = 126$ are close to those for Re$_\lambda = 204$. Note that we consider the difference of Fr is negligibly small. Figure 5 shows the power spectrum of number density fluctuations, $E_{np}(k)$, for Fr $= \infty$ and 0.145 at Re$_\lambda = 126$ and 204. The normalization of the horizontal and vertical axes is identical to that for Figure 2. For the case of St $< 1.0$, the
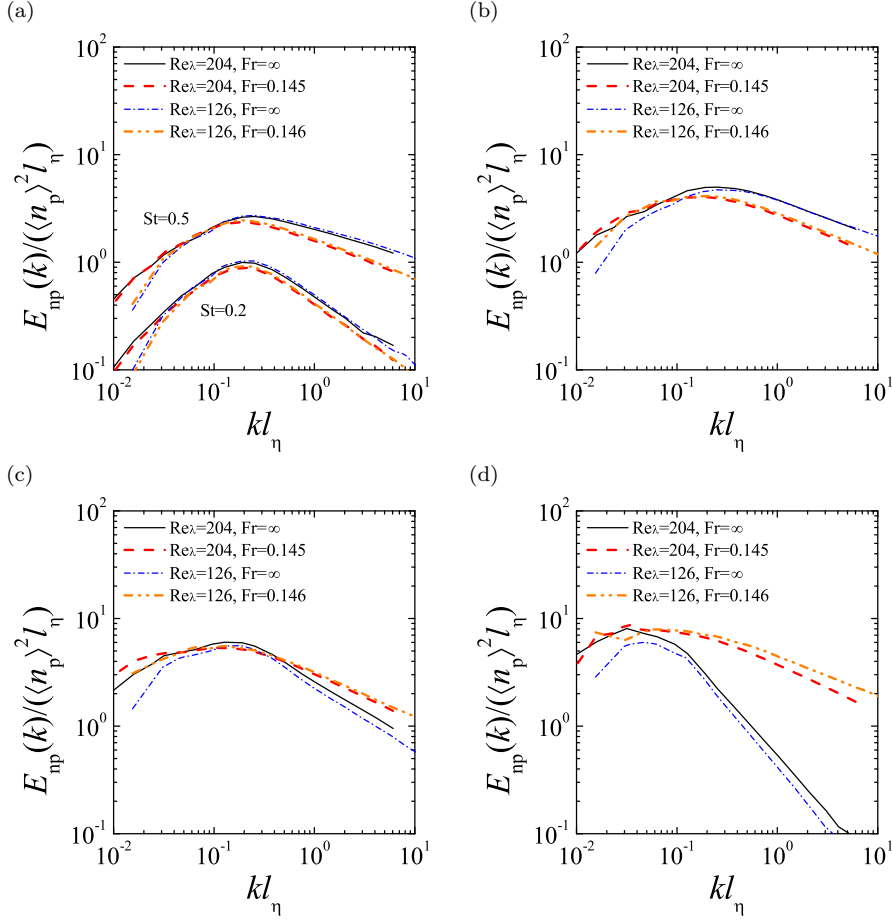
**Fig. 5** Power spectra of number density fluctuations considering gravitational settling for the case of (a) St < 1.0, (b) St = 1.0, (c) St = 2.0 and (d) St = 5.0 at $Re_\lambda = 126$ and 204.

$Re_\lambda$ dependence of the power spectrum is observed for $kl_\eta < 0.05$, where the settling influence is small. In contrast, the $Re_\lambda$ dependence is small for both Fr cases for $kl_\eta > 0.05$, where the settling influence is observed; i.e., the settling influence is not dependent on $\Sigma_v$. For the case of St = 1.0, the $Re_\lambda$ dependence of the power spectrum for Fr = $\infty$ is observed for $kl_\eta < 0.5$, whereas the $Re_\lambda$ dependence for Fr = 0.145 is observed only for $kl_\eta < 0.03$. This indicates that the $Re_\lambda$ dependence becomes insignificant under the presence of gravity. The $Re_\lambda$ dependence for St = 2.0 is similar to that for St = 1.0: the $Re_\lambda$ dependence for Fr = $\infty$ is observed for whole wavenumber range, whereas that for Fr = 0.145 is small. For the case of St = 5.0, the power spectrum for Fr = $\infty$ becomes lower for the whole wavenumber range as $Re_\lambda$ decreases. In contrast, the power spectrum for Fr = 0.145 becomes higher at large wavenumbers as $Re_\lambda$ decreases. In addition, the $Re_\lambda$ dependence at small wavenumbers

is insignificant. These are surprising results because the intensity of large-scale clustering is not dependent on large-scale eddies, whereas the intensity of small-scale clustering is strengthened by large-scale eddies. This indicates that DNSs at increased $\text{Re}_\lambda$ and consideration of anisotropy of clustering is necessary to clarify the settling influence on large St droplets since $\text{Re}_\lambda$ of turbulence in atmospheric clouds ($\text{Re}_\lambda \sim 10^3 - 10^4$) is much higher than the DNSs in this study. However, for small St droplets, we can evaluate the settling influence on the increment of the radar reflectivity factor in atmospheric clouds since the $\text{Re}_\lambda$ dependence is insignificant for $\text{St} \leq 2.0$.

### 4.3 Estimate of the increment of the radar reflectivity factor

The increments of the radar reflectivity factor, $Z$, due to turbulent clustering has been estimated from the power spectra. The increment of the radar reflectivity factor is given by

$$Z_{\text{cluster}}^{\text{dB}} - Z_{\text{random}}^{\text{dB}} = 10 \log_{10} \left[ 1 + \frac{2\pi^2 \langle n_{\text{p}} \rangle l_\eta}{\kappa^2} S(\kappa l_\eta) \right], \tag{13}$$

where $Z^{\text{dB}}$ is the value of $Z$ in units of decibels, defined as $Z^{\text{dB}}(\text{dBZ}) = 10 \log_{10} Z(\text{mm}^6/\text{m}^3)$. $S(\xi)$ is the normalized power spectrum given by $S(kl_\eta) = E_{\text{np}}(k)/(\langle n_{\text{p}} \rangle^2 l_\eta)$, where $\xi = kl_\eta$. For this estimate, the power spectra in Figure 2 (St = 1.0 and $\text{Re}_\lambda = 204$) was used. Since $g$, $\nu$ and $\rho_{\text{p}}/\rho_{\text{g}}$ were set to the same values as the DNS, the dimensional values of $\epsilon$ and the droplet radius, $r_{\text{p}}$, are given by the following equations:

$$\epsilon = \nu^{1/3} \left( \frac{\text{St} g}{f_{\text{T}} S_{\text{v}}} \right)^{4/3}, \tag{14}$$

$$r_{\text{p}} = \left( \frac{9\rho_{\text{g}}}{2\rho_{\text{p}}} \text{St} \right)^{1/2} \nu^{3/4} \epsilon^{-1/4}. \tag{15}$$

Thus, the increments of $Z$ for droplets with radius of $r_{\text{p}}$ were estimated for the case of corresponding $S_{\text{v}}$ and St. The increments of $Z$ under the absence of gravity were also estimated for the same $r_{\text{p}}$ for the reference. Note that the Stokes drag was assumed for these estimates. The volume fraction of cloud droplets, $\phi$, was set to $10^{-6}$, which corresponds to the condition in a dense cloud. The averaged number density, $\langle n_{\text{p}} \rangle$, is given by $\langle n_{\text{p}} \rangle = 3\phi/(4\pi r_{\text{p}}^3)$. This study focused on the microwave frequencies, $f_{\text{m}}$, of 2.8, 5.3 and 9.4 GHz, which are representative frequencies in frequency bands: S, C and X bands, respectively.

Figure 6 shows the increment of the radar reflectivity factor, $Z_{\text{cluster}}^{\text{dB}} - Z_{\text{random}}^{\text{dB}}$, for the case of St = 1.0. The droplet radius in the figure ranges from large cloud droplets (20 $\mu$m $\lesssim r_{\text{p}} \lesssim$ 40 $\mu$m) to small rain droplets ($r_{\text{p}} \gtrsim$ 40 $\mu$m). $\epsilon$ is approximately 100-1000 cm$^2$/s$^3$ in cumulonimbus and cumulus clouds and 50 cm$^2$/s$^3$ in stratocumulus clouds [28]. Thus, the surveyed range covers the typical values in the atmospheric turbulent clouds. The calculated
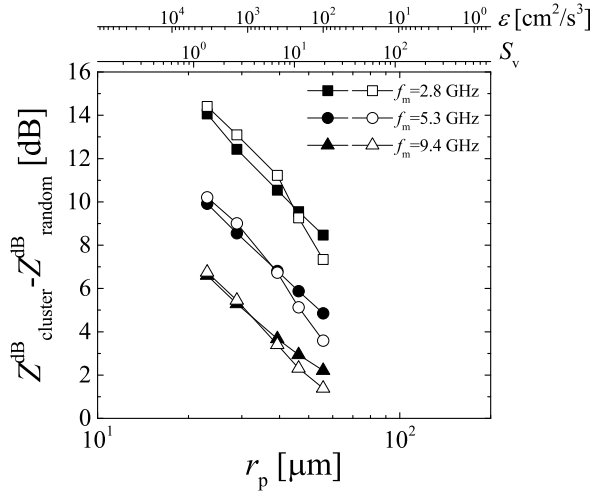
**Fig. 6** Increment of $Z^{\mathrm{dB}}$ for droplets of St = 1.0 at $\mathrm{Re}_\lambda = 204$. Black and open symbols indicate the cases of $g = 0$ and 9.8 m/s$^2$, respectively. The droplet volume fraction $\phi$ is $10^{-6}$.

$Z^{\mathrm{dB}}_{\mathrm{cluster}} - Z^{\mathrm{dB}}_{\mathrm{random}}$ is significantly larger than the observational error level, which is around 1 dB [5,6]. This means that the turbulent microscale clustering may lead to significant errors in radar observations [21]. $Z^{\mathrm{dB}}_{\mathrm{cluster}} - Z^{\mathrm{dB}}_{\mathrm{random}}$, i.e., the error due to clustering, increases as $f_{\mathrm{m}}$ decreases. For $r_{\mathrm{p}}$ smaller than 40 $\mu$m, the droplet gravitational settling tends to enlarge the error due to clustering, but within 1dB. For larger $r_{\mathrm{p}}$, the settling reduces the error due to clustering by larger than 1dB. These results indicate that the errors due to clustering for St = 1.0 reported in Matsuda et al. [21] may be overestimated for the small rain droplet range. It should be noted that the anisotropy of clustering can cause the dependence of the clustering influence on the zenith angle of the microwave transmission. The clustering influence on the radar reflectivity factor would be more significant for horizontally-transmitted microwaves and less significant for the vertically-transmitted microwaves.

## 5 Conclusion

This study has investigated the influence of gravitational settling on the spatial distribution of turbulent clustering droplets and the radar reflectivity factor by means of a three-dimensional direct numerical simulation (DNS) of particle-laden isotropic turbulence. The droplet distribution data obtained by the DNS have been used to calculate the power spectra of droplet number density fluctuations.

   Firstly, the authors have discussed the influence of gravity on turbulent clustering for the case where the Stokes number, St, is unity. The spatial droplet distribution clearly shows void areas and fine clustering structure.

The clusters becomes more extended in the vertical direction as the nondimensional terminal velocity based on the Kolmogorov velocity, $S_v$, increases. The power spectrum of droplet number density fluctuations becomes lower at large wavenumbers and becomes higher at small wavenumbers due to the gravitational settling. This settling influence increases as $S_v$ increases.

Secondly, the St dependence of the influence of gravitational settling has been investigated. The spatial droplet distributions for St $< 1.0$ under the presence of gravity (the Froude number is Fr $= 0.145$) is similar to those under the absence of gravity (Fr $= \infty$). The spatial droplet distributions for St $> 1.0$ under the presence of gravity show vertically extended clusters, which are not observed in the distribution under the absence of gravity. The power spectrum also shows the St dependence. The gravitational settling weakens the intensity of clustering at large wavenumbers for St $\leq 1.0$, whereas it significantly enlarges the intensity at large wavenumbers for St $> 1.0$.

The contribution of large-scale eddies to the settling influence on the power spectra have been also investigated by comparing the cases of two turbulent flows, where the Taylor-microscale-based Reynolds numbers, $Re_\lambda$, are different but the Kolmogorov scaling parameters are the same. For the case of St $\leq 2.0$, the dependence of the power spectrum on large-scale eddies is insignificant under the presence of gravity. On the other hand, for the case of St $= 5.0$, the intensity of large-scale clustering is not dependent on large-scale eddies, whereas the intensity of small-scale clustering is strengthened by large-scale eddies.

Finally, the radar reflectivity factors for the radar frequencies of 2.8, 5.3 and 9.4 GHz, which are representative frequencies in S, C and X bands, respectively, are estimated from the power spectrum under the conditions where St $= 1.0$ and the droplet volume fraction is $10^{-6}$. For droplets smaller than 40 $\mu$m, the gravitational settling enlarges the increment of the radar reflectivity factor due to turbulent clustering within 1 dB, whereas, for larger droplets, it reduces the increment by larger than 1 dB, which is the unavoidable error level in radar observations. Thus, the influence of gravitational settling can be significant under conditions of large gravitational settling velocity; i.e., weak energy dissipation rate.

# References

1. Ayala, O., Rosa, B., Wang, L.P.: Effects of turbulence on the geometric collision rate of sedimenting droplets. part 2. theory and parameterization. New J. Phys. **10**, 075,016 (2008)
2. Ayala, O., Rosa, B., Wang, L.P., Grabowski, W.: Effects of turbulence on the geometric collision rate of sedimenting droplets. part 1. results from direct numerical simulation. New J. Phys. **10**, 075,015 (2008)

3. Bec, J., Homann, H., Ray, S.: Gravity-driven enhancement of heavy particle clustering in turbulent flow. Phys. Rev. Lett. **112**, 184,501 (2014)
4. Bohren, C., Huffman, D.: Absorption and Scattering of Light by Small Particles. Wiley (1983)
5. Bringi, V., Chandrasekar, V., Balakrishnan, N., Zrnić, D.: An examination of propagation effects in rainfall on radar measurements at microwave frequencies. J. Atmos. Oceanic Technol. **7**, 829–840 (1990)
6. Carey, L., Rutledge, S., Ahijevych, D., Keenan, T.: Correcting propagation effects in c-band polarimetric radar observations of tropical convection using differential propagation phase. J. Atmos. Sci. **39**, 1405–1433 (2000)
7. Chen, L., Goto, S., Vassilicos, J.: Turbulent clustering of stagnation points and inertial particles. J. Fluid Mech. **553**, 143–154 (2006)
8. Clarke, A., Voight, B., Neri, A., Macedonio, G.: Transient dynamics of vulcanian explosions and column collapse. Nature **415**, 897–901 (2002)
9. Clift, R., Grace, J., Weber, M.: Bubbles, Drops, and Particles. Academic Press (1978)
10. Dombrovsky, L., Zaichik, L.: An effect of turbulent clustering on scattering of microwave radiation by small particles in the atmosphere. J. Quant. Spectro. Rad. Trans. **111**, 234–242 (2010)
11. Ellis, S., Vivekanandan, J.: Liquid water content estimates using simultaneous s and $k_a$ band radar measurements. Radio Sci. **46**, RS2021 (2011)
12. Gossard, E., Strauch, R.: Radar Observation of Clear Air and Clouds, *Developments in Atmospheric Science*, vol. 14. Elsevir, New York (1983)
13. Goto, S., Vassilicos, J.: Self-similar clustering of inertial particles and zero-acceleration points in fully developed two-dimensional turbulence. Phys. Fluids **18**, 115,103 (2006)
14. Grabowski, W., Vaillancourt, P.: Comments on "preferential concentration of cloud droplets by turbulence: Effects on the early evolution of cumulus cloud droplet spectra". J. Atmos. Sci. **56**, 1433–1436 (1999)
15. Gustavsson, K., Vajedi, S., Mehlig, B.: Clustering of particles falling in a turbulent flow. Phys. Rev. Lett. **112**, 214,501 (2014)
16. Hirt, C., Cook, J.: Calculating three-dimensional flow around structures. J. Comput. Phys. **10**, 324–340 (1972)
17. Kim, I., Elghobashi, S., Sirignano, W.: On the equation for spherical-particle motion: effect of reynolds and acceleration numbers. J. Fluid Mech. **367**, 221–253 (1998)
18. Knight, C., Miller, L.: First radar echoes from cumulus clouds. Bull. Am. Meteorol. Soc. **74**, 179–188 (1993)
19. Knight, C., Miller, L.: Early radar echoes from small, warm cumulus: Bragg and hydrometeor scattering. J. Atmos. Sci. **55**, 2974–2992 (1998)
20. Kostinski, A., Jameson, A.: On the spatial distribution of cloud particles. J. Atmos. Sci. **57**, 901–915 (2000)
21. Matsuda, K., Onishi, R., Hirahara, M., Kurose, R., Takahashi, K., Komori, S.: Influence of microscale turbulent droplet clustering on radar cloud observations. J. Atmos. Sci. **71**, 3569–3582 (2014)
22. Maxey, M.: The gravitational settling of aerosol particles in homogeneous turbulence and random flow fields. J. Fluid Mech. **174**, 441–465 (1987)
23. Maxey, M., Riley, J.: Flow due to an oscillating sphere and an expression for unsteady drag on the sphere at finite reynolds number. Phys. Fluids **26**, 883–889 (1983)
24. Okamoto, H., Nishizawa, T., Takemura, T., Kumagai, H., Kuroiwa, H., Sugimoto, N., Matsui, I., Shimizu, A., Emori, S., Kamei, A., Nakajima, T.: Vertical cloud structure observed from shipborne radar and lidar: Midlatitude case study during the mr01/k02 cruise of the research vessel mirai. J. Geophys. Res. **112**, D08,216 (2007)
25. Onishi, R., Baba, Y., Takahashi, K.: Large-scale forcing with less communication in finite-difference simulations of steady isotropic turbulence. J. Comput. Phys. **230**, 4088–4099 (2011)
26. Onishi, R., Takahashi, K., Komori, S.: Influence of gravity on collisions of monodispersed droplets in homogeneous isotropic turbulence. Phys. Fluids **21**, 125,108 (2009)
27. Park, Y., Lee, C.: Gravity-driven clustering of inertial particles in turbulence. Phys. Rev. E **89**, 061,004(R) (2014)

28. Pinsky, M., Khain, A., Krugliak, H.: Collision of cloud droplets in a turbulent flow. part v: Application of detailed tables of turbulent collision rate enhancement to simulation of droplet spectra evolution. J. Atmos. Sci. **65**, 357–374 (2008)
29. Rogers, R., Brown, W.: Radar observations of a major industrial fire. Bull. Amer. Meteor. Soc. **78**, 803–814 (1997)
30. Squires, K., Eaton, J.: Preferential concentration of particles by turbulence. Phys. Fluids A **3**, 1169–1178 (1991)
31. Stephens, G., Vane, D., Tanelli, S., Im, E., Durden, S., Rokey, M., Reinke, D., Partain, P., Mace, G., Austin, R., L'Ecuyer T. Haynes, J., Lebsock, M., Suzuki, K., Waliser, D., Wu, D., Kay, J., Gettelman, A., Wang, Z., Marchand, R.: Cloudsat mission: Performance and early science after the first year of operation. J. Geophys. Res. **113**, D00A18 (2008)
32. Valentine, G., Wohletz, K.: Numerical models of plinian eruption columns and pyroclastic flows. J. Geophys. Res. **94**(B2)
33. Wang, L., Maxey, M.: Settling velocity and concentration distribution of heavy particles in homogeneous isotropic turbulence. J. Fluid Mach. **256**, 27–68 (1993)
34. Woittiez, E., Jonker, H., Portela, L.: On the combined effects of turbulence and gravity on droplet collisions in clouds: A numerical study. J. Atmos. Sci. **66**, 1926–1943 (2009)
35. Yoshimoto, H., Goto, S.: Self-similar clustering of inertial particles in homogeneous turbulence. J. Fluid Mech. **577**, 275–286 (2007)